

## HiSST: 4th International Conference on High-Speed Vehicle Science Technology 22 -26 September 2025, Tours, France



# Thermal-Plasma Exposure Studies of Oxide/Oxide Ceramic Matrix Composites Under Varying Heat Flux and Environment

Hannah James<sup>1</sup>, Abhendra K. Singh<sup>2</sup>, Noel Clemens<sup>3</sup>, John S. Murray<sup>4</sup>

#### **Abstract**

Oxide/Oxide ceramic matrix composites (CMCs) have the potential to be used as multifunctional structures in hypersonic vehicles due to their load-bearing ability and thermal stability. However, ground-based testing is necessary to understand the material performance of candidate materials to the challenging hypersonic environments. Under hypersonic flight conditions, vehicle components may be exposed to temperatures approaching the melting point of alumina (approximately 2000°C), as well as to chemically active ionized gases. Therefore, it is necessary to understand the response of Oxide/Oxide CMCs to not just thermal loads, but also the added challenges of plasma environments in a variety of pressure states. In this research, an alumina-mullite based Oxide/Oxide CMC was exposed to various thermal plasma stream conditions intended to mimic the harsh conditions encountered in hypersonic flight. The samples were exposed for a duration of 5 minutes at heat fluxes between 80 and 100 W/ cm<sup>2</sup>. Samples were exposed at near vacuum (~3 torr) pressures at the HyMETS arc-jet facility at the NASA Langley Research Center, as well as under full atmospheric condition using the inductively coupled plasma generator located at the University of Texas at Austin. Physical degradation of the samples under atmospheric condition was more aggressive in comparison to those tested in nearvacuum environment. This also resulted in significant differences in the microstructural changes in the samples between the two environments.

**Keywords** oxide/oxide, ceramic matrix composites, plasma testing, microstructural characterization

#### 1. Introduction

In order to develop a reliable and robust hypersonic capability, extensive knowledge of material performance under uniquely aggressive conditions must be understood. Effective and relevant ground testing must be able to replicate, or at least approximate, a few key features of hypersonic aerothermodynamics: rapid heating rates, one-sided heating, appropriate chemically active species, lack of other contamination, and relevant test duration. [1] Thermal plasma testing heats gas to the extent that electrons dissociate from their source atoms and passes it in a controlled trajectory, thereby generating a hypersonic relevant test environment. [2]

Traditional hypersonic airspace is from 20 km to 130 km (66,000 ft to 433,000 ft)[3] which corresponds to 40 torr to near-vacuum conditions (approaching 0 torr). Hypersonic glide vehicles operate at lower altitudes with higher pressures, and any vehicle needing to travel to or away from ground level will also pass through these higher pressure environments. Therefore, the material response to thermal plasma

HiSST-2025-161 Page | 1 Thermal-Plasma Exposure Studies of Oxide/Oxide CMCs Copyright © 2025 by authors

Department of Mechanical Engineering, Baylor University, Waco, TX 76706, USA, hannah james@baylor.edu

<sup>&</sup>lt;sup>2</sup> Department of Mechanical Engineering, Baylor University, Waco, TX 76706, USA, abhen\_singh@baylor.edu

<sup>&</sup>lt;sup>3</sup> Department of Aerospace Engineering and Engineering Materials, The University of Texas at Austin, Austin, TX 78712, USA, clemens@mail.utexas.edu

<sup>&</sup>lt;sup>4</sup>Department of Aerospace Engineering and Engineering Materials, The University of Texas at Austin, Austin, TX 78712, USA, johnmurray94@utexas.edu

testing under a wide range of pressures is of interest.

One class of material that is gaining prominence for hypersonic applications is ceramic matrix composites (CMCs) [4]. These CMCs constitute ceramic or non-ceramic fibers embedded in a ceramic matrix. They are lighter than high temperature superalloys and can withstand temperatures higher than the melting point of these superalloys. At elevated temperatures the load bearing capability of CMCs is not significantly compromised and their specific strength, defined as strength per unit density, make them particularly attractive in aerospace applications. [5] Monolithic ceramics also have a high specific strength and temperature stability but are prone to brittle fracture. In comparison, CMCs improve the material toughness by introducing crack deflection mechanisms, allowing for quasi-ductile behaviour. Some of the common CMC systems with significantly high technology maturation level are SiC/SiC (silicon carbide fibers in a silicon carbide matrix), C/SiC (carbon fibers in a silicon carbide matrix) and Oxide/Oxide (alumina-based fibers in an alumina-based matrix).

While the mechanical performance and thermal stability of Oxide/Oxide CMCs are not as high as that of SiC/SiC or C/C composites, they have a few notable characteristics that make them desirable for regions of hypersonic vehicles away from the leading edge. Unlike SiC/SiC and C/SiC which contain a fully dense matrix and rely on finely tailored fiber coatings to provide a weak fiber/matrix interface for crack deflection mechanisms that give CMCs their fracture toughness, the pores in the oxide matrix provide numerous crack deflection points and an inherently weak fiber-matrix interface allows the fibers to slip under stress allowing for quasi-ductile behaviour and improved toughness. [6] Since both the fiber and matrix components in Oxide/Oxide CMCs are already present in their oxidized forms, they are resistant to additional oxidation that plague SiC/SiC and C/C CMCs. [7] This eliminates the need for prime-reliant environmental barrier coatings, and therefore significantly reduces the manufacturing cost and inspection needs of these components. Oxide/Oxide CMCs can be manufactured via pre-pregs or slurry infiltration methods, both of which have a high manufacturing maturity due to the analogies to PMC processing. This, along with the lack of need for high precision fiber coatings, makes Oxide/Oxide CMCs cheaper and easier to manufacture and maintain than SiC/SiC or C/C composites.

In this study, an alumina-mullite based Oxide/Oxide CMC was exposed to various thermal plasma stream conditions intended to mimic the harsh conditions encountered in hypersonic flight. The samples were exposed for a duration of 5 minutes at heat fluxes between 80 and 100 W/ cm². Post-test, the samples were characterized for physical degradation and microstructural changes.

## 2. Material and Test Methodology

#### 2.1. Material

CMC laminates with an alumina-mullite matrix (AM/N720) were obtained from COI Ceramics (San Diego, CA). The reinforcement in the CMC is 1500D, 8-harness satin fabric of Nextel 720 fiber. The 18 ply laminates had a stacking sequence of  $[(0/90)_4/0]_s$ , and an average thickness of 4.05 mm. According to the manufacturer, the laminates contained a matrix of approximately 80% alumina and 20% mullite, a fiber volume fraction of 44%, a porosity of 24% and a final bulk density of 2.6 g/cm<sup>3</sup>. The laminates were machined into 25 mm diameter disks using a water jet to prepare for exposure in the plasma jet systems.

## 2.2. Plasma Exposure

Samples were exposed to thermal plasma under near vacuum conditions at the HyMETS Facility located at the NASA Langley Research Center in Hampton, VA. The system in enclosed in a vacuum chamber and steady state conditions of around 2.8 torr were maintained during the duration of the test. Heat fluxes of 80, 90, and 100 W/cm² were used for durations of 5 minutes with laboratory air as the carrier gas. The HyMETS facility is designed so that the plasma stream flowed horizontally, with samples positioned perpendicular to the flow stream using a sting arm, as shown in Fig 1. A silicon carbide fixture surrounded the sample and screwed to the sting base. The front face temperature was measured using a multispectral pyrometer (FMP2/2X, FAR Associates, Macedonia, OH, USA) through a view window in the chamber. A fiber optic cable was mounted to a table near the HyMETS system and aimed through a viewing window to collect data from a path passing directly in front of the sample surface.

One spectrometer (HR, Ocean Optics, Orlando, Florida, USA) captured data between 200 nm and 420 nm and another Ocean Optics USB2000+, captured data from 195nm to 880nm.

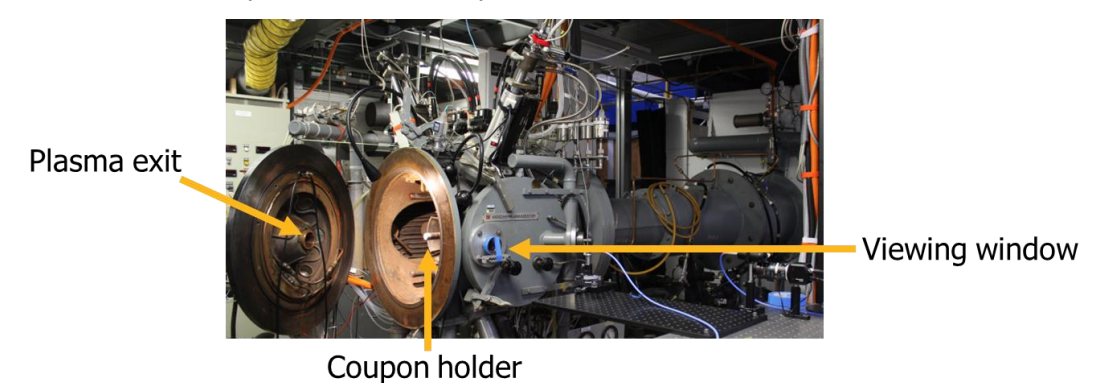


**Fig. 1** HyMETS Test facility at NASA Langley Research Center with the chamber door open showing the sting arm with coupon holder.

Samples were exposed to thermal plasma under full atmospheric pressure conditions using the Inductively Coupled Plasma (ICP) system located at the University of Texas at Austin in Austin, TX. This system is not enclosed in any chamber, and so samples experience ambient atmospheric pressure and humidity during exposure. Heat fluxes of 80, 90, and 100 W/cm² were used for durations of 5 minutes with laboratory air as the carrier gas. The ICP facility is designed so that the plasma stream flows up from below the sample, as shown in Fig 2. Samples were positioned perpendicular to the flow stream using a high temperature adhesive, Graphi-Bond 551-RN-MV, to bond the sample to the sting. To prolong the life of the adhesive, an alumina ceramic paste, Resbond 940HT, was placed around the edge of the CMC coupon, enclosing the Graphi-Bond adhesive and shielding it from the high temperature air. The front face temperature was measured using a pyrometer (IGA 740-LO, Impac, Denver, CO) reflected on a nearby mirror. An emission spectrometer (HR2, Ocean Optics, Orlando, FL, USA) captured wavelengths between 250 nm and 1100 nm.

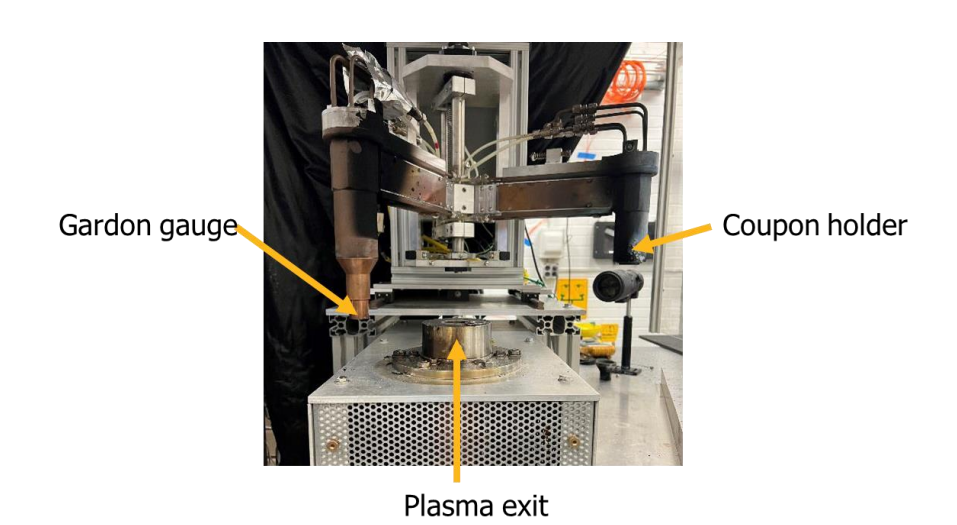


**Fig 2.** ICP system at the University of Texas at Austin showing the plasma exit, coupon holder, and some system diagnostics.

#### 2.3. Post-Test Sample Evaluations

After the samples were removed from the plasma jet systems, they were inspected physically and characterized microstructurally using a variety of techniques. Optical images of the surface and polished cross sections of the samples were taken using a 3D measurement system (VR-3000, Keyence, Osaka, Japan) and a digital microscope (VHX-7000, Keyence, Osaka, Japan). Scanning Electron Microscopy (SEM) of both sample surfaces and polished cross sections were done using a Focused Ion Beam Scanning Electron Microscope Versa 3D (FIB-SEM, FEI Company, Hillsboro, OR, USA). X-Ray diffraction

measurements were taken of the sample surface with a Siemens XRD Diffraktometer D500 (Siemens AG, Munich, Germany) with a copper  $K\alpha$  tube with settings of 30 mA, 40 kV, and a 0.2° step at 1.5 s/step between 2° and 70°.

#### 3. Results and Discussion

#### 3.1. Material Response During Test

Video recordings of the side profiles of the samples were taken during the testing. No samples tested under near vacuum conditions showed any debris liberated from the surface during the plasma impingement. Representative image from the 100W/cm² tests are shown in Fig. 3. In contrast, under ambient atmospheric pressure, glowing debris was visible near the sample surface at all heat flux conditions, with higher heat fluxes eliciting significantly more visible debris. A representative image from the 100W/cm² case is shown in Fig. 3b. The surface of the sample appeared static and unmoving in samples tested under near vacuum conditions but physically active in the samples tested in ambient pressure conditions, showing a thin layer of softened or molten material present on the sample surface.

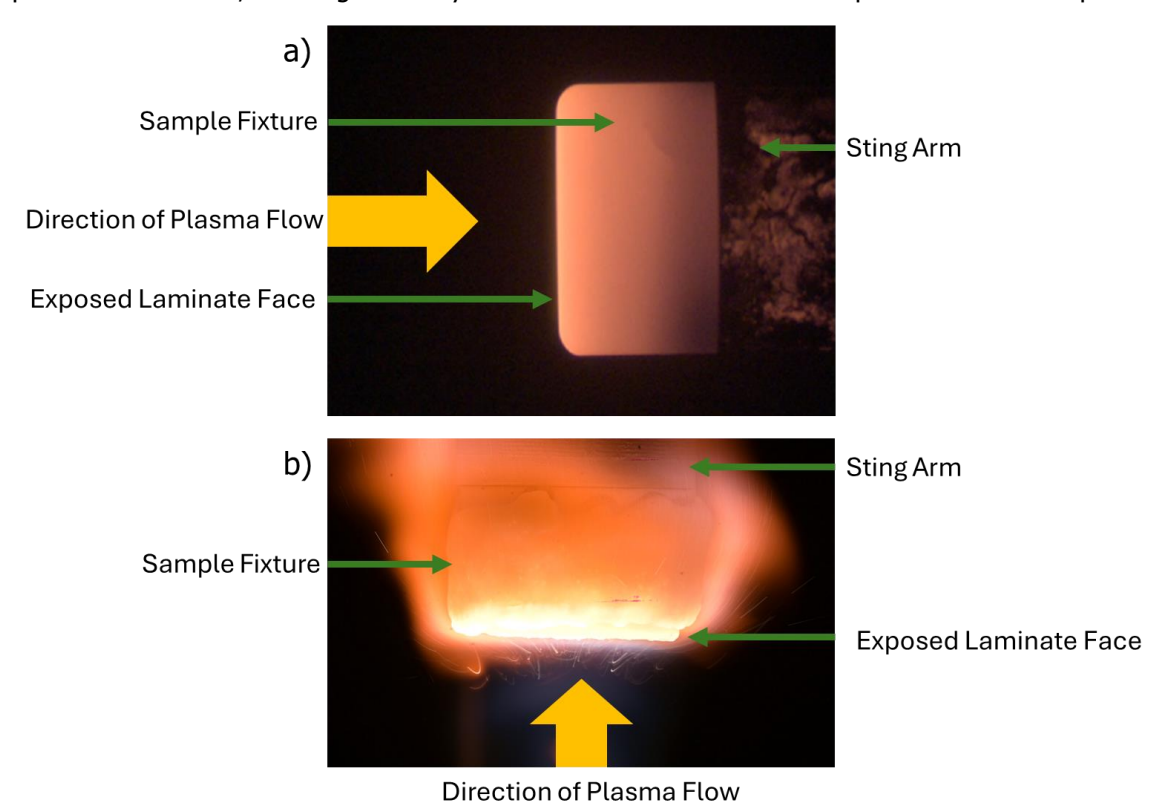


**Fig 3.** Still images from video recordings during exposure at 100 W/cm<sup>2</sup> at a) near vacuum conditions and b) ambient atmospheric pressure conditions. In a) the plasma flow proceeds from left to right and in b) in the plasma flow proceeds from bottom to top. No debris is visible in the near vacuum conditions of a), but a significant amount is visible in the ambient pressure conditions of b).

The recorded temperature measurements for the front face temperature from the various pyrometers are shown in Fig 4. For samples tested under near vacuum conditions, an elevated temperature was reached very rapidly after exposure began with a steady state temperature of about  $2000^{\circ}$ C was reached by around 1 minute into the sample exposure. High levels of noise were seen in the first few seconds of exposure due to the uneven initial heating patterns. However, for samples tested under atmospheric conditions, a more gradual ramp to final temperature of around  $1500^{\circ}$ C was observed over time that varied between 1-2 minutes. The data logging software experienced a failure during the second run at  $80 \text{ W/cm}^2$ , so data from only one run of that condition is available.

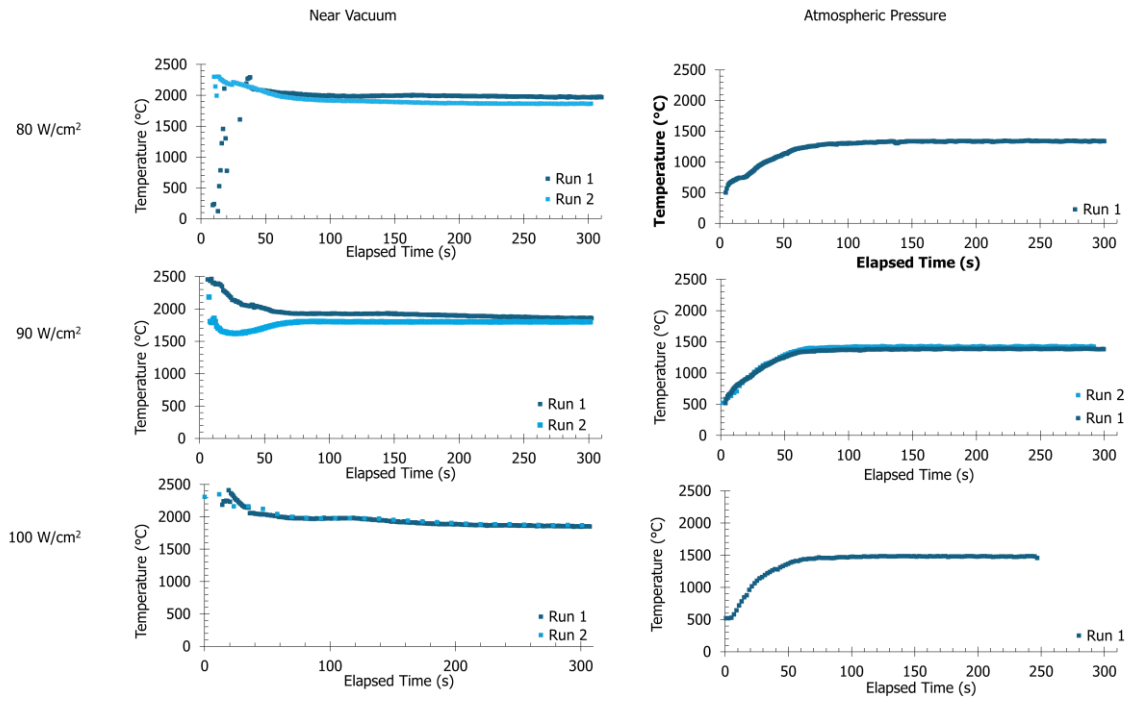


**Fig 4.** Plots of temperature over time during plasma exposure under near vacuum and ambient pressure conditions at 80 W/cm², 90 W/cm² and 100 W/cm².

Emission spectroscopy showed the presence of characteristic oxygen excitation peaks in all samples regardless of testing condition, but also characteristic aluminium peaks only in samples tested under ambient pressure conditions.

#### 3.2. Physical and Microstructural Characterization Results

Optical microscopy images of a representative sample surface of each condition are shown in Figs. 5 and 6. In Fig 5, the overall morphology of the samples can be seen, showing the flat, crips edges of the samples tested under near vacuum conditions and the rounded and exaggerated edges of those tested under ambient atmosphere. Fig 6 contains a higher magnification image of each sample showing the surface texture. In the samples tested under near vacuum conditions, remnants of a weave pattern were still visible on the sample surface, but the top layers began to slough off and form ribbons. All three heat flux levels were relatively consistent with each other. However, under ambient atmospheric conditions the surface showed much more distortion. In the samples exposed to 80 W/cm² a weave pattern can still be resolved but is significantly distorted from the original pattern. The samples at 90 W/cm² and 100 W/cm² showed no remaining weave and instead the top surface was transformed into a relatively uniform pebbly texture across the surface. These observations are consistent with the surface activity observed during the video recordings of the exposure.

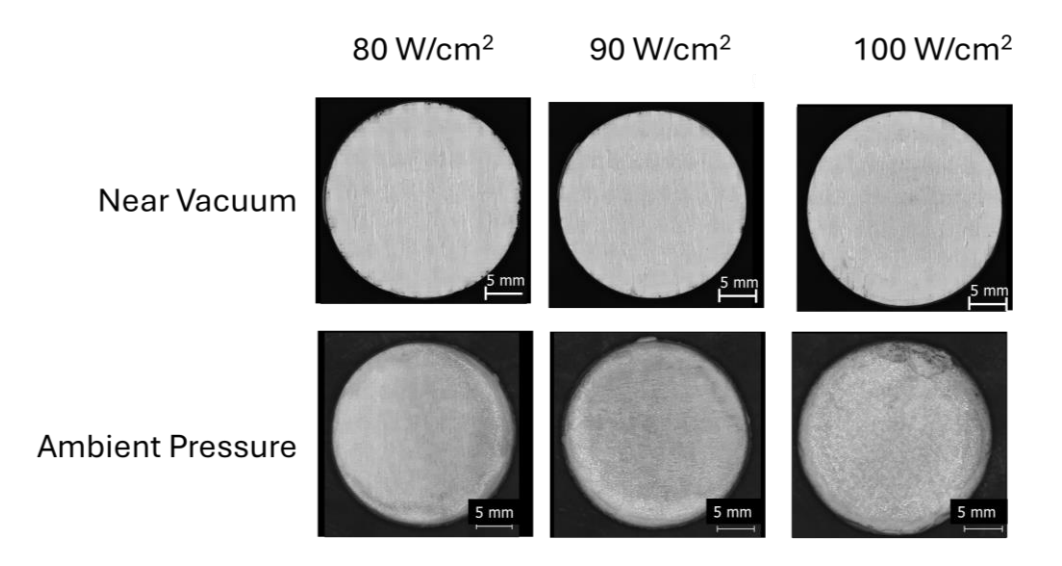
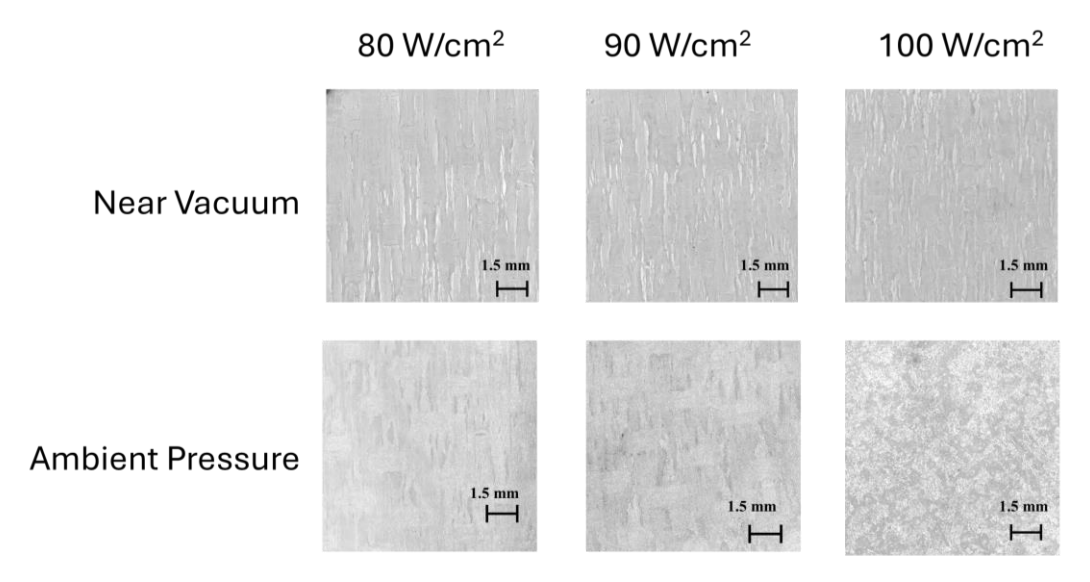


Fig 5. Optical microscopy images of the full exposed surface of samples exposed to plasma flow.



**Fig 6.** Optical microscopy images of the exposed surface of samples exposed to plasma flow showing the remaining texture.

X-Ray diffraction was used to measure the overall phase composition of the surface, and the profiles are shown in Fig. 7. For all the samples tested in near vacuum conditions, peaks from both alumina and mullite phases were present in approximately the same ratios as in the as-manufactured control sample. No significant change between the three heat flux conditions was observed. Both alumina and mullite peaks were visible in samples tested at 80 W/cm² under ambient atmospheric conditions as well. However, above 90 W/cm², only the characteristic peaks corresponding to the presence of alumina are visible, indicating that the mullite has either been removed from the sample surface, or masked by an alumina phase.

**Fig 7.** XRD profiles of samples exposed to plasma under a) near vacuum conditions and b) ambient pressure conditions.

One sample from each condition was cut through the center of the disk and the cross section mounted and polished. Images from a Keyence digital microscope appear in Fig 8 for the samples exposed at 90 W/cm². The thickness change of each laminate is listed in Table 1. For samples tested in near vacuum conditions, this was measured with a thickness gauge. The presence of adhesive made that not practical for the atmospheric pressure samples, so those were measured via microscopy. In an as-manufactured sample, there are crisp boundaries between the fiber and matrix visible. After exposure to thermal plasma, the fibers nearest the impingement region blur, showing fusing of the fibers with the matrix, indicating the laminate is losing some of its distinctiveness as a composite and will behave more like a monolithic ceramic. For samples tested under near vacuum conditions, as the heat flux increased, the depth of this fused zone increased, as listed in Table 1. However, for samples tested under ambient pressure conditions, no fibers were visible right at the impingement region and fusing of the fibers and matrix were visible throughout the entire laminate thickness.

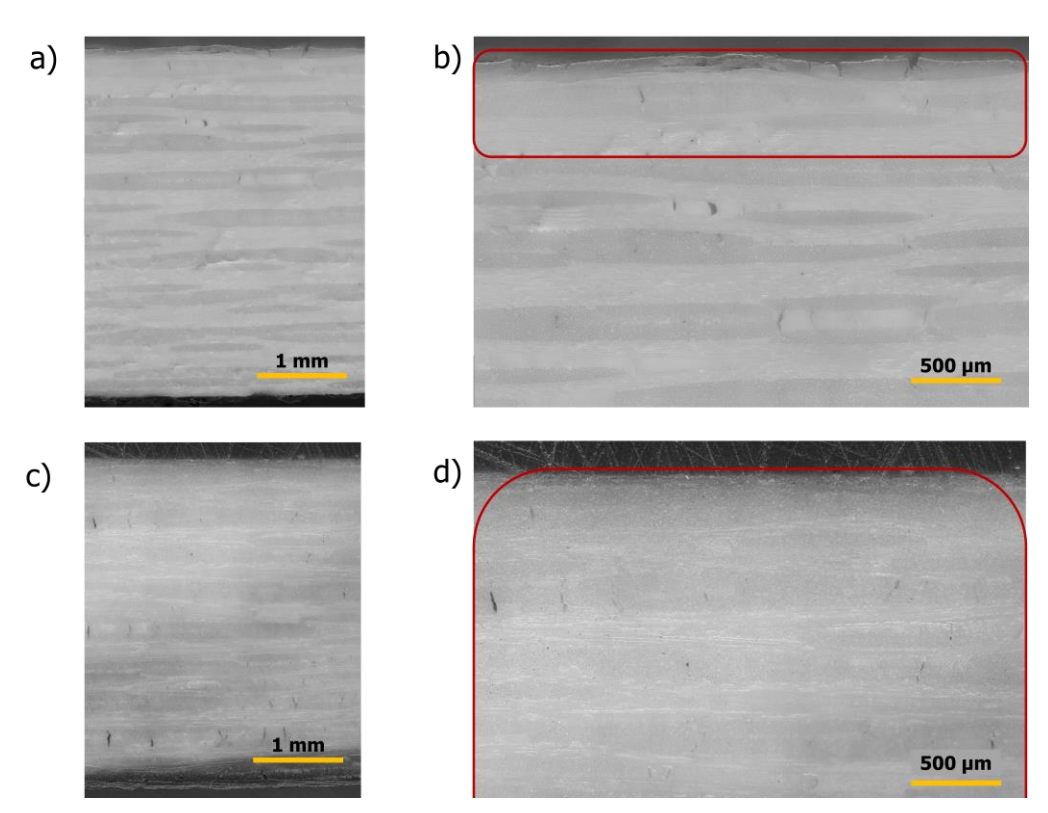


**Fig 8.** Optical microscopy images of polished cross sections of samples exposed to thermal plasma at 90 W/cm² with the impinged surface on the top of each image. a) full laminate thickness after testing in near vacuum test conditions; b) higher magnification image of the sample exposed in near vacuum test conditions with the region of visible matrix and fiber fusing indicated in red; c) full laminate thickness after testing in ambient pressure conditions; b) higher magnification image of the sample exposed in ambient pressure conditions with the region of visible matrix and fiber fusing indicated in red, continuing through the full sample thickness.

	Table 1	. Thickness	loss and	1 fiber	fusina	in sam	nles after	plasma exposure.
--	---------	-------------	----------	---------	--------	--------	------------	------------------

	Near Vacuu	m Conditions	Ambient Atmospheric Conditions		
Heat Flux	Thickness Loss	Depth of Fiber Fusing	Thickness Loss	Depth of Fiber Fusing	
80 W/cm <sup>2</sup>	1.5%	250 μm	4.7%	Full Thickness	
90 W/cm <sup>2</sup>	1.1%	500 μm	5.4%	Full Thickness	
100 W/cm <sup>2</sup>	2.7%	1200 μm	12.9%	Full Thickness	

The fusing of the fiber and matrix was investigated more thoroughly using scanning electron microscopy. Fig 9 shows images of the fiber and matrix near both the surface where the plasma impinged and near the back surface away from the plasma. For samples tested under near vacuum conditions, significant distortion of the fiber/matrix interface is visible on the impingement side and the distinction between the matrix and the fiber is difficult to delineate. However, on the back side, crisp clean boundaries are visible in all cases. In contrast, under ambient pressure conditions samples tested at 90 w/cm² and 100 W/cm² had no fibers visible at all near the top surface because all the material in this region had melted during exposure and then resolidified as the sample cooled. In the sample exposed at 80 W/cm², indications of previous fiber locations were visible, but no clear distinct fibers with visible grains. Lower magnification images of this region are shown in Fig. 9 to illustrate the lack of fibers regardless of imaging area. On the back side of the laminates, fibers were visible but with significant distortion and fusing with the matrix.

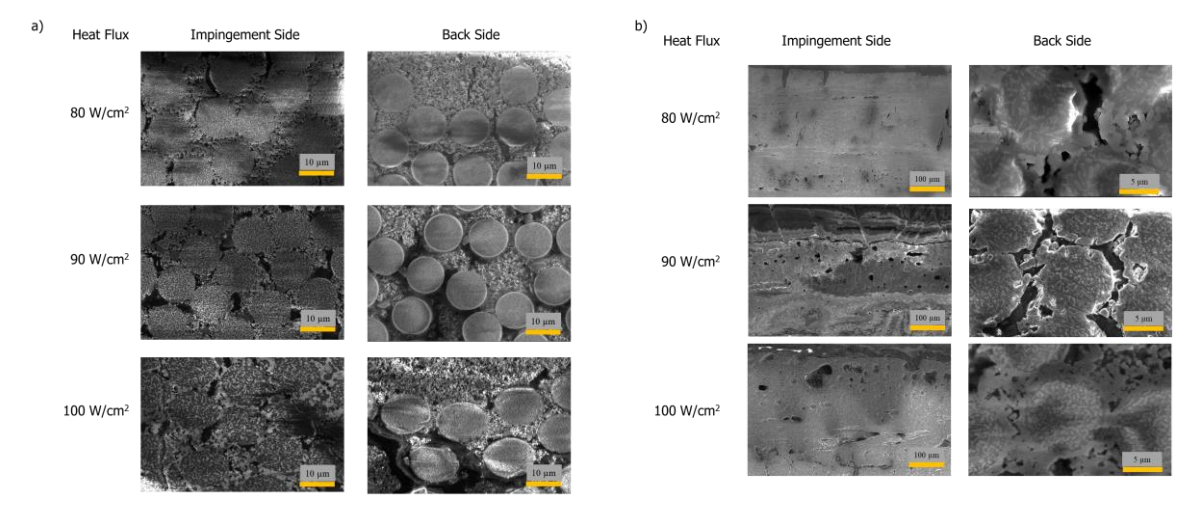


**Fig 9**. SEM images of the Nextel 720 fiber embedded in an alumina mullite matrix after exposure to thermal plasma both near the surface that was impinged by plasma and near the opposite surface. a) shows images from samples exposed under near vacuum conditions and b) shows samples exposed under ambient pressure conditions.

Higher magnification images in Fig. 10 show the grain texture within the fibers. For samples tested under near vacuum conditions, the grains significantly coarsened within the fibers. With increasing heat flux, the grain size increased near the impingement side, but only slightly coarsened on the back side far from the impingement region.

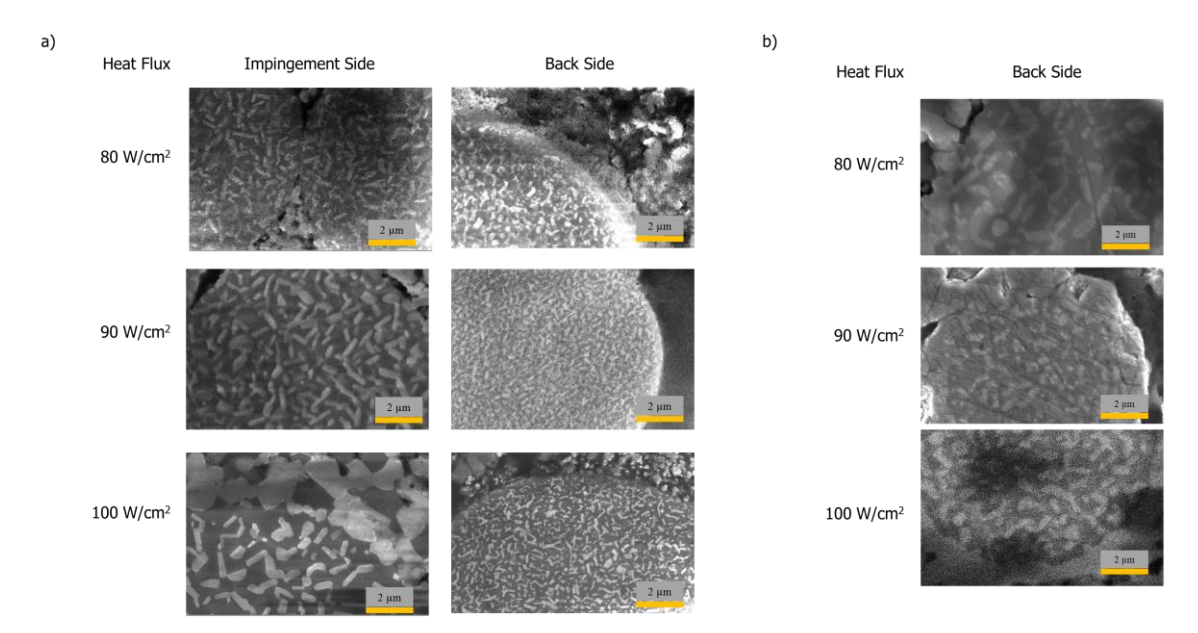


**Fig 10.** SEM images of the Nextel 720 fiber embedded in an alumina mullite matrix after exposure to thermal plasma in a) near vacuum conditions and b) ambient atmospheric conditions.

In each image within Fig. 10, the length of the major axis of 25 different columnar grains was measured and the average length plotted in Fig 11. In the samples tested in near vacuum conditions, the grain size steadily increased with heat flux, with the impingement side grain sizes being significantly larger than the back side. In samples tested in ambient pressure conditions, no measurement could be taken on the impingement side since no fiber remnants were visible. On the back side, there was a significant size increase in the grain size as compared to an as-manufactured laminate for all cases, but the magnitude did not directly correlate with heat flux.

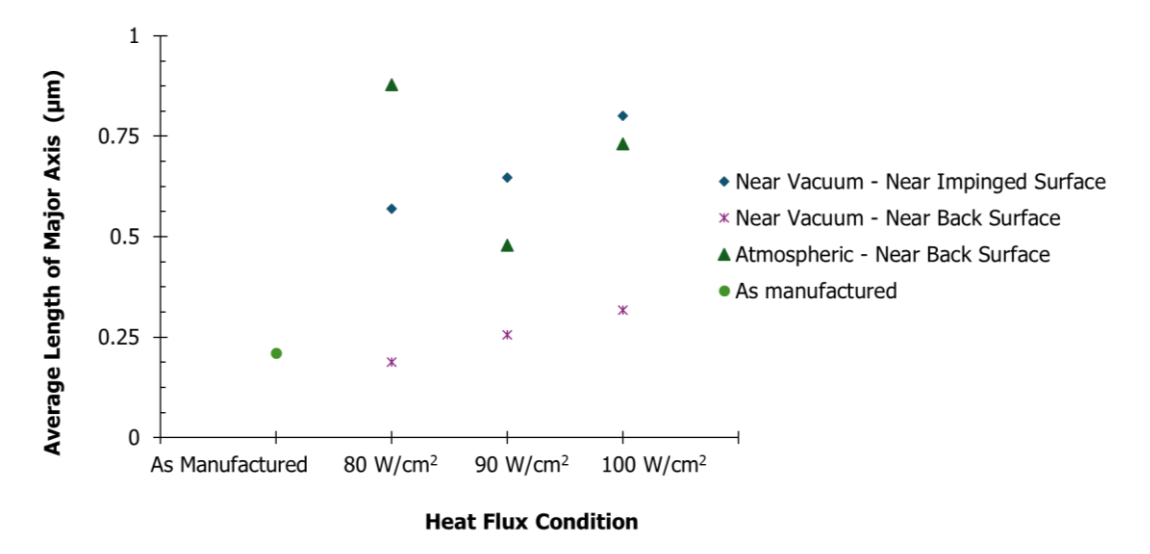


**Fig 11.** Plot of the length of the major axis of the columnar  $\alpha$ -alumina grains within the Nextel fibers as a function of sample condition.

#### 4. Conclusions

The results of the plasma exposure testing described in this study make it clear that heat flux is not the only parameter that must match the flight profile to ensure accurate ground-based testing. Most realistic hypersonic flight trajectories will include portions of both high altitude and low altitude travel, and so plasma testing under various pressure conditions is necessary to replicate flight behaviour and therefore predict the service life of vehicle components. In particular, this testing showed a dramatic difference in the material response regarding:

- Surface temperature and response during exposure
- Thickness loss measured via physical thickness gauges and optical microscopy
- Surface phase composition measured via XRD
- Surface texture observed through optical microscopy
- Fusing of fibers with surrounding matrix
- Grain growth within fibers

These observed microstructure changes have the potential to dramatically effect the mechanical performance of the laminates and therefore their durability during service.

#### References

- Boyd, I.: Modeling of Plasma Formation in Rarefied Hypersonic Entry Flows. 45th AIAA Aero Sciences Meeting and Exhibit, Am. Inst. of Aeronaut. Astronaut., (2007). https://doi.org/10.2514/6.2007-206
- 2. Boulos, M.I, Fauchais, P., Pfender, E.: Thermal Plasmas. Springer, Boston, (1994)
- 3. Lau, R.C.: "Hypersonic Airspace: How Hypersonic Weapons Conquer and Define the Realm Between Airspace and Space," OTH: Over the Horizon. Available: https://overthehorizonmdos.wpcomstaging.com/2022/02/14/hypersonic-airspace-how-hypersonic-weapons-conquer-and-define-the-realm-between-airspace-and-space/ (2022) Accessed 31 Jan. 2024.
- 4. Glass, D.: Ceramic matrix composite (CMC) thermal protection systems (TPS) and hot structures for hypersonic vehicles, 15th AIAA International Space Planes and Hypersonic Systems and Technologies Conference, Am. Inst. of Aeronaut. Astronaut, (2008) https://doi.org/10.2514/6.2008-2682.
- 5. Ohnabe, H., Masaki, S., Onozuka, M., Miyahara, K., Sasa, T.: Potential application of ceramic matrix composites to aero-engine components, Composites Part A (1999), https://doi.org/10.1016/S1359-835X(98)00139-0.
- 6. Ramachandran, K., Bear, J.C., Jayaseelan, D.D.: Oxide-Based Ceramic Matrix Composites for High-Temperature Environments: A Review. Adv. Eng. Mater. (2025) https://doi.org/10.1002/adem.202402000.
- 7. Courtright, E.L. "Engineering Property Limitations of Structural Ceramics and Ceramic Composites Above 1600°C," in Proceedings of the 15th Annual Conference on Composites and Advanced Ceramic Materials: Ceramic Engineering and Science Proceedings (1991) https://doi.org/10.1002/9780470313848.ch9.
- 8. Rozenbaum, O., Meneses, D.D.S., Auger, Y., Chermanne, S., Echegut, P.: A spectroscopic method to measure the spectral emissivity of semi-transparent materials up to high temperature. Rev. Sci. Instrum., (1999) https://doi.org/10.1063/1.1150028.

HiSST-2025-161 Hannah James, Abhendra K. Singh